Photoexcitation of a one-dimensional polarization-inverted domain from the charge-ordered ferroelectric ground state of (TMTTF)$_2$PF$_6$

T. Yamaguchi,[1] K. Asada,[2] H. Yamakawa,[2] T. Miyamoto,[2] K. Iwano,[3] T. Nakamura,[4] N. Kida,[2] and H. Okamoto[2,5]

[1]*Institute of Materials Structure Science, High Energy Accelerator Research Organization (KEK), 1-1 Oho, Tsukuba 305-0801, Japan*
[2]*Department of Advanced Materials Science, The University of Tokyo, 5-1-5 Kashiwa-no-ha, Chiba 277-8561, Japan*
[3]*Graduate University for Advanced Studies, Institute of Materials Structure Science, High Energy Accelerator Research Organization (KEK), 1-1 Oho, Tsukuba 305-0801, Japan*
[4]*Institute for Molecular Science, Myodaiji, Okazaki 444-8585, Japan*
[5]*AIST-UTokyo Advanced Operando-Measurement Technology Open Innovation Laboratory, National Institute of Advanced Industrial Science and Technology, Chiba 277-8568, Japan*

We theoretically revealed that a weak photoexcitation achieves the electric polarization-inversion with approximately 18% of all the charges, which was interpreted as a superimposition of multiexciton states, from the charge-ordered ferroelectric ground state of (TMTTF)$_2$PF$_6$ at absolute zero temperature. Regarding a relative change of electric polarization ($\Delta P/P$), the photoexcitation corresponds to 36%, which is much larger than $\Delta P/P$ of other typical organic materials. The photoexcitation of $\Delta P/P \sim 36\%$ corresponds to the single peak of the optical conductivity in the low-energy region, which was also observed at 10 K. Therefore, the value of $\Delta P/P \sim 36\%$ can be achieved in the early stage of the ultrafast photoinduced dynamics of the material. This fact is useful not only for applications of this material and other analogous materials in optical devices, but also for research toward controlling electric polarizations by light, which is one of the recent attracting issues in photoinduced phase transition phenomena. Theoretical calculations are based on a quarter-filled one-dimensional effective model with appropriate parameters and 50 unit cells.

I. INTRODUCTION

Studies on controlling the purely electronic phase transitions occurring immediately after a photoexcitation from the ground state of matter have been attracting attention because such photoinduced phase transitions (PIPTs) regulate the macroscopic properties of matter on an ultrafast timescale [1,2]. Once such electronic PIPTs are applied to organic ferroelectric materials, the electric polarization can be tuned in the regime of femtoseconds. Because of notable properties such as mechanical flexibility, disposability, and inexpensiveness, organic materials are increasingly being applied to electronic and optical devices. In this regard, flexible tuning of a light-induced electric polarization in the order of femtoseconds is one of the most attractive challenges in the field of PIPTs, recently.

So far, as one of the light sources to easily create and control such devices, visible light (light) is actually most convenient. In this regard, PIPTs induced by light have actively been studied. For instance, a light-induced ultrafast insulator-metal transition has been observed in a quasi-two-dimensional molecular solid, α-(BEDT-TTF)$_2$I$_3$ (BEDT-TTF = bis(ethylenedithiolo)tetrathiafulvene) [3]. Because the material undergoes ferroelectric polarization in the charge-ordered (CO) ground state [4,5], this transition is regarded as a photoinduced disappearance of the polarization. A photoexcitation of a nonpolarized state from a ferroelectric polarized ground state has been reported for a quasi-one-dimensional

molecular solid, TTF-CA (tetrathiafulvene-chloranil) [6]. Very recently, a photoinduced polarization suppression was observed in croconic acid and it was regarded as a light-induced polarization inversion of protons [7]. However, at present we are not aware of any experimental achievement regarding a light-induced electronic ferroelectric inversion.

Theoretical works on PIPTs of organic materials with charge orders also have been actively studied, as summarized in Ref. [8], for instance. Those works investigated and explained the experiments, some of which were previously introduced. Namely, polarization modulations with or without phase transitions from the CO phases by light have been theoretically reported. However, the possibility of photoinduced polarization modulations of (TMTTF)$_2$X (TMTTF = tetramethyltetrathiafulvene) has not been theoretically discussed yet, even though the materials with particular anion X have the ferroelectric CO phases as their ground states.

(TMTTF)$_2$X F$_6$ (X = P, As, Sb, Ta) is known as one of the quasi-one-dimensional quarter-filled organic conductors and it has rich physical phases [9–17]. In particular, the bulk electronic ferroelectricity of (TMTTF)$_2$PF$_6$ caused by finite charge disproportion δ_{co} has been experimentally depicted [18–22] in both a CO phase and spin-Peierls (SP) phase. According to Ref. [10], the CO and SP phase of (TMTTF)$_2$PF$_6$ have been achieved below 67 and 19 K, respectively. In our study, representing ρ_{rich} (ρ_{poor}) as the rich (poor) value of the charge of the two closest TMTTF molecules forming a dimer, $\delta_{co} \equiv \rho_{rich} - \rho_{poor} \geqslant 0$ is treated.
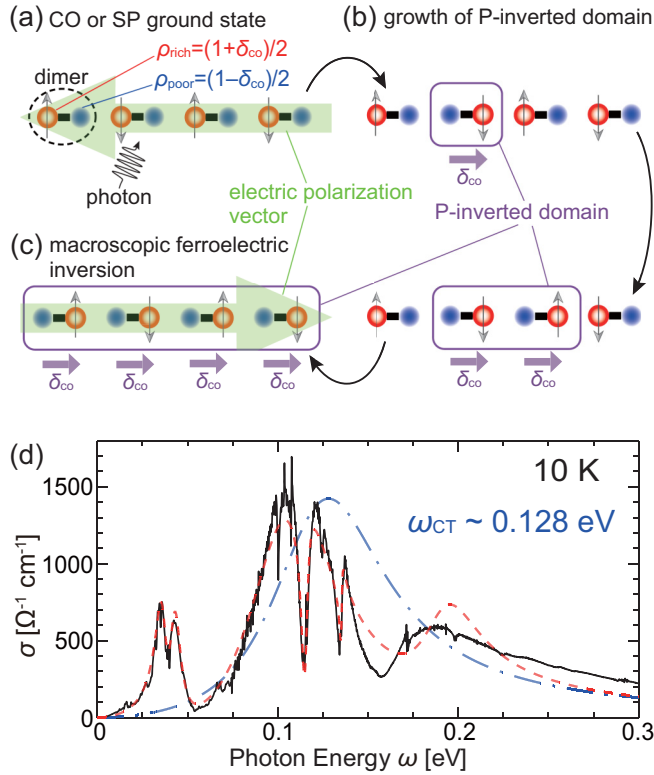
FIG. 1. (a)–(c) Schematics of the CO or SP ground state and photoexcited states of $(TMTTF)_2PF_6$. The circle and up (down) arrows on the circles represent a molecular orbital of a TMTTF molecule and up (down) spins, respectively. (d) Optical conductivity spectrum of $(TMTTF)_2PF_6$ with the electric field polarized parallel to the *a* axis at 10 K (solid line) and the fitting curve (dashed line). The chained line shows the calculated spectrum with resonant energy 0.128 eV.

The observed finite δ_{co} values in $(TMTTF)_2PF_6$ below 67 K [23–25] indicate that the SP phase also has the characteristics of the CO phase of $(TMTTF)_2PF_6$.

In the theoretical works on other materials in terms of the PIPTs [26–29], the photoexcitations associated with the collective excitations of charges, namely, multiexcitons, have been discussed. When these concepts are applied to $(TMTTF)_2PF_6$, photoexcitations of the one-dimensional (1D) polarization (P)-inverted domain from its ferroelectric ground state are strongly expected by following processes, as schematically shown in Figs. 1(a)–1(c), with defining the total number of dimers as $D = 4$ (eight sites). Here, note that a dimer corresponds to a unit cell. First, one dimer is photoexcited by a single photon (weak photoexcitation) from the ferroelectric CO ground state, and then a 1D P-inverted domain is generated. This roughly corresponds to an inversion of a single electric dipole moment [see the upper panel of Fig. 1(b)]. Next, the 1D domain broadens due to collective excitations (multiexcitons) as displayed in the lower panel of Fig. 1(b). Thus, sufficiently strong collective excitations will possibly lead to a huge growth of the 1D domain, namely, a production of a 1D macroscopic P-inverted domain. Consequently, when charges with $D\delta_{co}$ move from the CO ground state in the entire system, the

bulk ferroelectric inversion can be achieved [see Fig. 1(c)]. Note that all the above processes are induced by electrons, and the timescale of forming such a 1D P-inverted domain is much faster than the typical relaxation time originating from phonons.

To realize such macroscopic polarization inversion in $(TMTTF)_2PF_6$, the most important issue is to know accurately the nature of the low-energy optical excitations of electrons. In particular, optical conductivities include the information of the early stage of the weakly photoinduced dynamics just after the injection of a single photon into the system. So far, several optical conductivities of $(TMTTF)_2PF_6$ and other analogous materials have already been observed [30–32]. However, little is known about the pure electronic excitations related to the peaks of the optical spectra. In this regard, we first observed the optical conductivity of $(TMTTF)_2PF_6$ at 10 K (in the SP phase) and estimated $\omega_{CT} \sim 0.128$ eV as the pure electronic excitation energy, as shown in Fig. 1(d). Details of this measurement are explained in Appendix A. A single crystal of $(TMTTF)_2PF_6$ was prepared by a previous method [33,34]. The complete structure of our spectrum, shown as a solid line in Fig. 1(d), is very similar to the previous spectra of $(TMTTF)_2PF_6$ at 20 K (in the CO phase) [30,31]. This suggests that the pure electronic photoexcited state from the CO ground state can be physically considered as almost the same as that from the SP ground state.

In the following sections of this article, we introduce our theoretical analyses, particularly of the optical conductivity spectrum in $(TMTTF)_2PF_6$, and discuss the nature of the observed peak structure exhibited as a chained line in Fig. 1(d). In addition to this, we theoretically investigate whether our idea of a 1D P-inverted domain as roughly sketched in Figs. 1(a)–1(c) actually can be realized or not. Here, we note again that, as discussed above, those theoretical analyses reveal the electronic photoexcitations in the early stages of the ultrafast dynamics immediately after a single photon injection. Throughout this paper, we consider $\hbar = e = 1$ and lattice constant $= 1$ for simplicity.

II. FORMULATION

We now consider a dimerized 1D chain model with even N_s sites, which is a quarter-filled hole system. An equal population of spins ($N_\uparrow = N_\downarrow = N_s/4$) is assumed at absolute zero temperature. Using model-specified parameters V_{eff} and V_{edge}, our Hamiltonian H is written as follows:

$$H \equiv H_t + H_{Coulomb} + V_{eff} \sum_{j:even} n_j + V_{edge} n_{N_s}, \quad (1)$$

$$H_t = -\sum_{j,\sigma} t_j [c^\dagger_{j+1,\sigma} c_{j,\sigma} + c^\dagger_{j,\sigma} c_{j+1,\sigma}], \quad (2)$$

$$H_{Coulomb} = U \sum_j n_{j,\uparrow} n_{j,\downarrow} + V \sum_j n_{j+1} n_j, \quad (3)$$

where $c^{(\dagger)}_{j,\sigma}$ denotes the annihilation (creation) operator of a hole with spin $\sigma = \uparrow, \downarrow$ at the jth site, and $n_j \equiv n_{j,\uparrow} + n_{j,\downarrow}$ represents the jth site density operator ($n_{j,\sigma} \equiv c^\dagger_{j,\sigma} c_{j,\sigma}$). j denotes a highest occupied molecular orbital (HOMO) of a TMTTF molecule. Because each dimer has three electrons in

HOMOs and the band consists of HOMOs, the system is regarded as a (third) quarter-filling in terms of holes (electrons). The dimerization of the system is treated in term t_j, where $t_j \equiv t_1$ (t_2) for even (odd) j represents an inter (intra)-dimer transfer integral. From a density functional theory (DFT) calculation of $(TMTTF)_2PF_6$ at 4 K [35], we select $t_1 = 0.1686$ eV and $t_2 = 0.1912$ eV. Referring to the reported Coulomb repulsive interaction strengths for $(TMTTF)_2X$-type compounds [16,36], we basically use $U = 1$ eV and $V = 0.2$–0.6 eV.

Within the framework of the linear response theory, optical conductivity with respect to photon energy $\omega > 0$ and infinitesimally small positive number η is written as

$$\sigma_1(\omega) = -\frac{1}{N_s\omega}\text{Im}\left[\langle\psi_0|J\frac{1}{\omega + i\eta + E_0 - H}J|\psi_0\rangle\right], \quad (4)$$

where

$$J \equiv i\sum_{j,\sigma} t_j[c^\dagger_{j+1,\sigma}c_{j,\sigma} - c^\dagger_{j,\sigma}c_{j+1,\sigma}] \quad (5)$$

denotes a charge-current operator, E_0 represents the ground-state energy, and $|\psi_0\rangle$ is the ground-state wave function. For computational problems, $\eta/t_2 = 0.05$ (~ 0.01 eV) is used.

$\sigma_1(\omega)$ is computed by the dynamical density-matrix renormalization group (dynamical DMRG or DDMRG) scheme [37] under the open boundary condition (OBC). In general, although the numerical accuracy of a DMRG [38] calculation under the OBC is better than that under the periodic boundary condition (PBC), the charges around the edges under the OBC are rich because of breaking of the translational symmetry of the system. Although several approaches have been proposed to avoid this unphysical problem to some extent [39–41], in this study, we apply potential V_{edge} at the edge site [42] as one of its solutions and fix $V_{edge} = 50t_2$. The value of $V_{edge} = 50t_2$ is chosen as small as possible to satisfy the condition that E_0 of all the calculations hardly depend on V_{edge} due to unpermitted $V_{edge} \to +\infty$. Because the charge at the N_sth site is poor at the V_{edge}, the CO ground state considered here has a charge-rich (poor) site at the first (N_sth) site.

Our calculations are done with $N_s = 100$ (50 dimers). This value is enough large to satisfy with $N_s + 1 \sim N_s$ (the system size under the OBC) and to quantitatively estimate the bulk properties, although finite-size effects still remain in the order of $1/N_s$. The truncation number of density matrices is 400 in our all the DMRG and DDMRG calculations. All the sweep processes stopped when the numerical relative error of adjacent sweeps was less than 10^{-6} for E_0 and 10^{-3} for $\sigma_1(\omega)$.

We introduce the number of photoexcited charges N_{ex} [26] to discuss the relationship between a photoexcited state and the collective excitations of the charges. Using

$$|\psi(\omega)\rangle \equiv \frac{1}{\mathcal{N}}\frac{\eta}{(\omega + E_0 - H)^2 + \eta^2}J|\psi_0\rangle, \quad (6)$$

where $\mathcal{N}$ denotes a normalization factor of $|\psi(\omega)\rangle$,

$$N_{ex} \equiv \sum_{j:even}[\langle\psi(\omega)|n_j|\psi(\omega)\rangle - \langle\psi_0|n_j|\psi_0\rangle] \quad (7)$$

can be defined. Here, $\langle\phi|n_j|\phi\rangle$ ($\phi = \psi_0, \psi(\omega)$) corresponds to the site density at the jth site. Because we consider weak photoexcitations and a single photon injected into the system, $N_{ex} > 1$ denotes the occurrence of collective excitation. We also theoretically estimate the charge disproportion by

$$\delta_{co} \equiv \frac{1}{2}\sum_{j=49,51}|\langle\phi|n_j - n_{j+1}|\phi\rangle| \quad (0 \leqslant \delta_{co} \leqslant 1). \quad (8)$$

Because the center of the system gives the most accurate expectation values of localized operators by DMRG calculations under the OBC, we choose the system centered two dimers for calculating δ_{co}.

III. RESULTS AND DISCUSSIONS FOR $V_{eff} = 0$

We first show the theoretical results for $\sigma_1(\omega)$ using several realistic values for V in the case of $V_{eff} = 0$ (the conventional model) as shown in Fig. 2(a). As can be seen, a single peak of $\sigma_1(\omega)$ appears around the so-called dimerization gap of $\omega_d \equiv 2|t_1 - t_2| \sim 0.045$ eV, which corresponds to the minimum gap of free dispersions. Although this is supported by another DDMRG calculation [43] with a different parameter set [44,45], ω_d deviates from ω_{CT}. In addition, in the ground
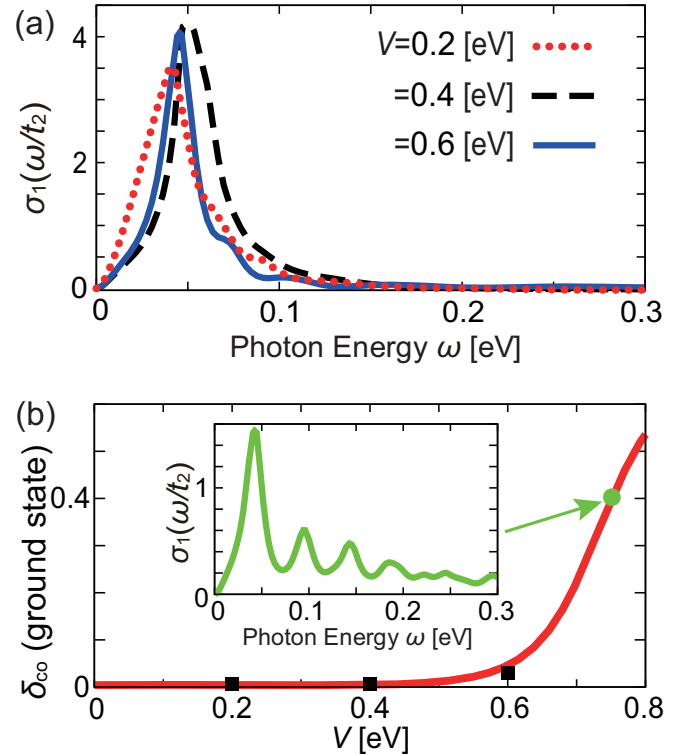

FIG. 2. DMRG and DDMRG calculations for $V_{eff} = 0$ at $N_s = 100$. (a) Results for $\sigma_1(\omega/t_2)$. (b) δ_{co} of ground states. The parameter set of $t_1 = 0.20$ eV, $t_2 = 0.22$ eV, and $U = 2.2$ eV [46] is used only for calculations presented in this figure. δ_{co} values at the ground states for the parameter sets in (a) are plotted as filled squares for comparison. The inset is $\sigma_1(\omega/t_2)$ with $t_1 = 0.20$ eV, $t_2 = 0.22$ eV, $U = 2.2$ eV [46], and $V = 0.75$ eV for giving $\delta_{co} = 0.40$ in the ground state.

state, $\delta_{co} \sim 0.03$ is the maximum value in our calculation and does not reproduce $\delta_{co} = 0.40$, which was recently observed in an x-ray diffraction experiment at 30 K [25]. To reproduce $\delta_{co} = 0.40$, we recalculate δ_{co} as a function of V by utilizing a different parameter set estimated by another DFT calculation [46], namely, $U = 2.2$ eV, $t_1 = 0.20$ eV, and $t_2 = 0.22$ eV. The results are shown in Fig. 2(b), and we determine the best parameter of $V = 0.75$ eV. However, the complete structure of $\sigma_1(\omega)$ at $V = 0.75$ eV shown in the inset of Fig. 2(b) deviates from our observation at 10 K, as shown as the chained line in Fig. 1(d). In particular, the broad spectral shape significantly differs from the observed single peak, and we interpret the former feature as the exaggerated collectiveness of the excitations, which will be discussed subsequently. Thus, the conventional model ($V_{eff} = 0$) should be modified to some extent.

IV. RESULTS AND DISCUSSIONS FOR $V_{eff} \neq 0$

As an alternative approach for reproducing $\delta_{co} = 0.40$ [25], we introduce the V_{eff} term, which increases δ_{co}. Next, we employ $V/t_2 = 3.138$ ($V = 0.6$ eV) because it gives the maximum value, $\delta_{co} \sim 0.03$, in the ground state with $V_{eff} = 0$. We find $V_{eff}/t_2 = 0.086$ as the best value. As one of the origins of V_{eff}, we consider an electron-intramolecular vibration (EIMV) coupling [47–49] and try to reproduce the

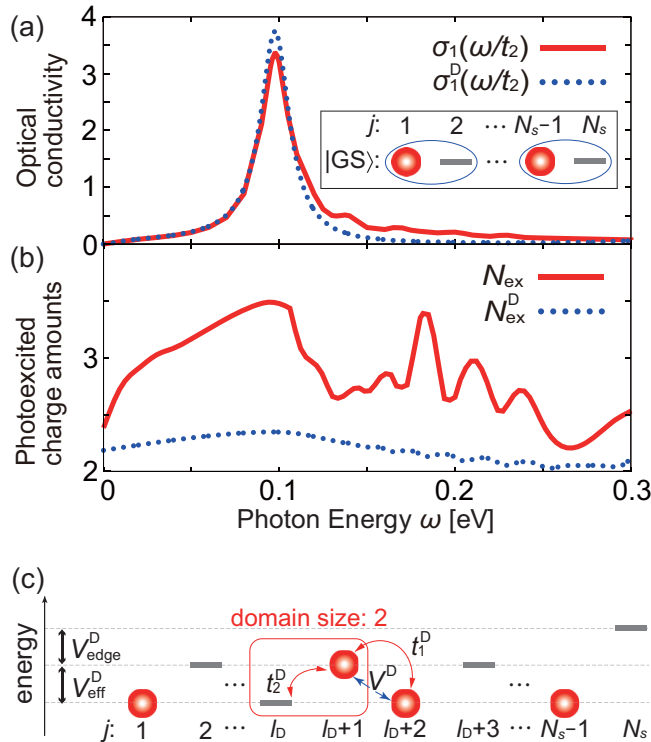value of $V_{eff}/t_2 = 0.086$ in Appendix B 1. V_{eff} under the EIMV coupling is physically related to an effective potential representing the deformed molecular orbitals with $\delta_{co} \neq 0$. Here we comment on two more possible origins of V_{eff} associated with a two- (2D) or three-dimensional (3D) effect. An origin of a 2D effect is a Coulomb interaction acting on interchains. This is because Ref. [25] reported the 2D CO pattern of $(TMTTF)_2PF_6$ forming a 2D Wigner crystal at 30 K (in the CO phase). A 3D dipolar interaction is another origin, and it generates a depolarization field which depends on a 3D crystallographic shape. However, that field possibly stabilizes the polarization inversions to some extent. These complicated origins beyond a 1D system, however, will be discussed using more coarse-grained 2D or 3D models in our future paper.

The results of $\sigma_1(\omega)$ and N_{ex} with $V/t_2 = 3.138$, $V_{eff}/t_2 = 0.086$ are shown in Figs. 3(a) and 3(b), respectively. A sharp peak structure of $\sigma_1(\omega)$ can be seen to arise at around 0.10 eV, and this is clearly closer to ω_{CT} than ω_d. Furthermore, in Fig. 3(b), $N_{ex} \geqslant 2$ denotes that all the photoexcited states are the collective excitations of the charges and that a maximum value of $N_{ex} \sim 3.5$ appears at the sharp peak of $\sigma_1(\omega)$. As mentioned above, because $N_{ex} = \delta_{co}N_s/2 = 20$ corresponds to the bulk ferroelectric inversion, a polarization inversion over $3.5/\delta_{co} \sim 9$ unit cells ($3.5/20 \sim 18\%$ of all the charges)

FIG. 3. Calculations of $V_{eff} \neq 0$ at $N_s = 100$. (a), (b) DDMRG results of $\sigma_1(\omega)$, N_{ex} (solid lines) and $\sigma_1^D(\omega)$, N_{ex}^D by using our effective model (dotted lines). The inset of (a) is a schematic of $|GS\rangle$ in our effective model ($\delta_{co} = 1$). The circles and horizontal bars represent single charges and empty sites, respectively. (c) Schematic energy diagram of basis $|l_D, n\rangle$ with $n = 1$ and odd l_D. Only $|l_D : \text{odd}, n\rangle$ states are generated from intradimer hopping.
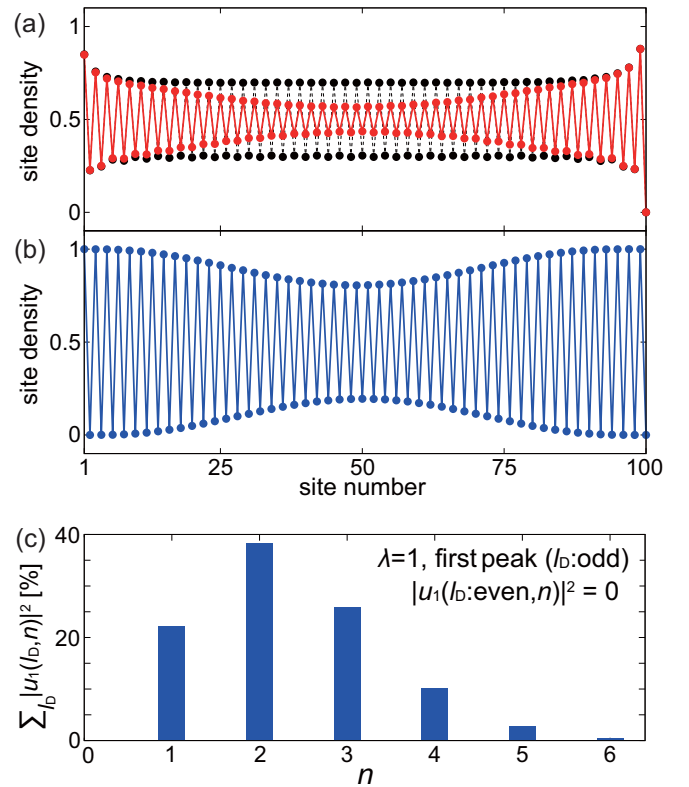
FIG. 4. Properties of the photoexcited states at the peak of both $\sigma_1(\omega)$ and $\sigma_1^D(\omega)$ with $V_{eff} \neq 0$ at $N_s = 100$. (a) Site densities of the ground state (dotted line) and peak state (solid line) by the DDMRG method. (b) Site density of the peak state by our effective model. (c) Probability weights of the peak state by our effective model with respect to basis $|l_D, n\rangle$ for odd l_D. Probability weights for even l_D are absent.

can be achieved at the peak. To understand this collective excitation at the peak, we compare the site density of this peak state with that of the ground state in Fig. 4(a), and we find that δ_{co} decreases to approximately 0.13. This reduction in δ_{co} at the peak can be explained by two scenarios as follows. The photoexcited state at the peak partially includes a 1D P-inverted domain ($\delta_{co} \to -\delta_{co} \neq 0$) or dimer–Mott (DM)-insulating state ($\delta_{co} = 0$). In this article, we discuss only the former scenario by extending the effective model proposed in Refs. [26,27]. However, the above case of a DM-insulating state is insignificant, as discussed in Appendix B 2. This indicates that the peak state is still in the CO phase.

V. EFFECTIVE MODEL ANALYSIS FOR $V_{eff} \neq 0$

Our effective model under the OBC assumes the CO ground state obtained by the DMRG method ($\delta_{co} = 0.40$) as the charge localized limit, $\delta_{co} = 1$. The normalized ground-state wave function of this model, $|GS\rangle$, contains the charges only at the odd sites. Using the site density operator at the jth site, n_j^D, $\langle GS|n_j^D|GS\rangle = 1$ (0) for odd (even) j is satisfied as approximately sketched in the inset of Fig. 3(a). All the physical parameters also differ from those of H, and in particular, U vanishes in this model. When we define the basis $|l_D, n\rangle$ as the photoexcited state with a single 1D P-inverted domain continuously arranged in $2n$ sites with starting site l_D, the Hamiltonian of our effective model is described as

$$H_{dmn} \equiv - \sum_{l_D,n} t(l_D)[|l_D - 2, n+1\rangle\langle l_D, n| + \text{H.c.}]$$
$$- \sum_{l_D,n} t(l_D)[|l_D, n+1\rangle\langle l_D, n| + \text{H.c.}] \qquad (9)$$
$$+ \sum_{l_D,n} E(n)|l_D, n\rangle\langle l_D, n|,$$

where $t(l_D) \equiv t_1^D$ (t_2^D) for even (odd) l_D and

$$E(n) = \begin{cases} nV_{eff}^D + V_{edge}^D & (l_D = N_s - 2n + 1) \\ V^D + nV_{eff}^D & \text{(otherwise)}. \end{cases} \qquad (10)$$

Here, t_1^D (t_2^D) denotes an inter (intra)-dimer transfer integral. A schematic is shown in Fig. 3(c). Eigenenergies ε_λ and eigenstates $|\lambda\rangle$ $[1 \leqslant \lambda \leqslant (N_s/2)^2]$ satisfy $H_{dmn}|\lambda\rangle = \varepsilon_\lambda|\lambda\rangle \equiv \sum_{l_D,n} u_\lambda(l_D, n)|l_D, n\rangle$. Introducing the charge-current operator of this model J^D and $|\psi_1\rangle \equiv J^D|GS\rangle = i \sum_{l_D}(-1)^{l_D - 1}t(l_D)|l_D, 1\rangle$, the optical conductivity of this model is defined as

$$\sigma_1^D(\omega) = \frac{\eta}{N_s\omega} \sum_\lambda \frac{|\langle\lambda|\psi_1\rangle|^2}{(\omega - \varepsilon_\lambda)^2 + \eta^2} \equiv \frac{\langle\psi_1|\omega\rangle}{\mathcal{C}N_s\omega}, \qquad (11)$$

where $\mathcal{C}$ is determined by $1 = \langle\omega|\omega\rangle$ and the number of photoexcited charges,

$$N_{ex}^D \equiv \sum_{j:even}\left[\langle\omega|n_j^D|\omega\rangle - \langle GS|n_j^D|GS\rangle\right]$$
$$= \sum_{j:even}\langle\omega|n_j^D|\omega\rangle, \qquad (12)$$

can be also defined.

To relate the nature of the photoexcited state at the peak of $\sigma_1(\omega)$ to that of $\sigma_1^D(\omega)$, $\sigma_1^D(\omega)$ and N_{ex}^D should resemble $\sigma_1(\omega)$ and N_{ex}, respectively, most accurately. Employing $N_s = 100$, $t_2^D = t_2 = 0.1912$ eV, $V_{edge}^D/t_2^D = 50$, and $\eta/t_2^D = 0.05$, we succeeded in reproducing $\sigma_1(\omega)$ of $V_{eff} \neq 0$ with $t_1^D/t_2^D = 0.600$, $V^D/t_2^D = 2.615$, and $V_{eff}^D/t_2^D = 0.528$ as shown in Fig. 3(a). Although N_{ex}^D underestimates N_{ex} with $V_{eff} \neq 0$ as illustrated in Fig. 3(b), the overall behavior of N_{ex}^D is qualitatively consistent with that of N_{ex} in terms of the collective excitation of the charges ($N_{ex}^D > 2$) in the entire ω region. $N_{ex}^D \sim 2.3$ is the maximum value and appears at the peak of $\sigma_1^D(\omega)$. In addition, although the site density at the peak as displayed in Fig. 4(b) differs from that obtained by the DDMRG scheme in Fig. 4(a) owing to our assumption of $\delta_{co} = 1$ at the ground state, the dip structure located around the center of the system is consistent with the DDMRG result. According to the above results, the peak state of $\sigma_1(\omega)$ can be regarded as that of $\sigma_1^D(\omega)$, which corresponds to the $\lambda = 1$ eigenstate with $\sum_{l_D=odd}\sum_{1\leqslant n\leqslant 6}|u_1(l_D = \text{odd}, n)|^2 \sim 99.9\%$ and $u_1(l_D = \text{even}, n) = 0$, as shown in Fig. 4(c). This implies that the photoexcited state is generated by an intradimer hopping and consists of the superposition of the 1D P-inverted domains over 1–6 unit cells.

Regarding the case of $U = 2.2$ eV mentioned already, we find much larger N_{ex} values at the peaks of the corresponding spectrum [inset of Fig. 2(b)], which are in the range 6–9. Because these large N_{ex} values indicate a strong collectiveness of the charge excitations [26], we determined that the present system lies in the category of modest collectiveness.

Here, we briefly discuss the lifetime of a 1D P-inverted domain by utilizing an effective model as introduced in this section. The effective model can be extended to include 1D multi-P-inverted domains. If plural 1D P-inverted domains unite into a single 1D P-inverted domain, this process can stabilize a 1D macroscopic P-inverted domain with huge size. Then, a generation of a long-lived 1D electronic ferroelectric inversion domain is expected by a weak photoexcitation. Theoretical investigations of this interesting situation, however, are positioned as one of our future works.

VI. CONCLUSIONS

To conclude, we have investigated a photoexcited state from the CO ground state of (TMTTF)$_2$PF$_6$. We found that the calculated spectrum based on a quarter-filled 1D effective model ($V_{eff} \neq 0$) reproduces the experimental spectrum of the CO ground state. We clarified that the electronic component of the optical conductivity had a single significant peak at around 0.10 eV and that the photoexcited state at the peak could be regarded as a superimposed state of the 1D P-inverted domains with a modest collectiveness.

For the photoexcited state at the peak, approximately 18% of the charges in the system contribute to the 1D P-inverted domains generated by a single photon (weak photoexcitation). Regarding a relative change of electric polarization ($\Delta P/P$), this corresponds to $\Delta P/P \sim 36\%$, which is clearly much larger than $\Delta P/P \sim 2$–10% of other ferroelectric organic materials for a weak photoexcitation [7,50]. Here, P denotes the initial polarization. As usual, observing the second-harmonic generation (SHG) signals with an irradiating THz pulse,

$\Delta P/P \sim \Delta I_{SHG}/(2I_{SHG})$ can be estimated, where $I_{SHG} \propto P^2$ is satisfied. However, we cannot succeed in that observation in the CO ground state of $(TMTTF)_2PF_6$ at present, so the experimental check of $\Delta P/P \sim 36\%$ still remains as one of our future problems.

Here, we consider that the difficulty of observing $\Delta P/P \sim 36\%$ may be a smallness of P. This causes a low signal-to-noise (S/N) ratio and difficulty in observing the SHG signals. In general, a typical electronic ferroelectric P value of organic materials is smaller than that value of inorganic materials, such as the maximum value of $P \sim 30\ \mu C/cm^2$ of $LuFe_2O_4$ [51]. For instance, $P \sim 6.3\ \mu C/cm^2$ of TTF-CA, which is one of the quasi-1D molecular materials, has been experimentally reported in its ionic (electronic ferroelectric polarized) phase [52]. $\Delta P/P \sim 0.75\%$ is also reported in that phase by observing the SHG signals [53]. For a 2D ferroelectric molecular solid, α-$(BEDT$-$TTF)_2I_3$, $\Delta P/P \sim 1.31\%$ has been observed in the CO phase [5]. According to Ref. [5], a DFT calculation of estimating $P \sim 1\ \mu C/cm^2$ in that CO phase was performed, although the value was experimentally undetermined. Judging from the above situations of organic solids, we believe that the SHG signals corresponding to $\Delta P/P \sim 36\%$ will be also observed.

Injecting multiphotons into the system (strong photoexcitation) can enhance $\Delta P/P$ and possibly generate a 1D macroscopic P-inverted domain spreading over the entire system, which is simply the achievement of bulk ferroelectric inversion. Therefore, examining strongly photoexcited effects is one of the crucial and challenging future tasks. However, our results adequately showed that $(TMTTF)_2PF_6$ could be a promising material for applications in optical switching devices and memories in the context of such macroscopic manipulation of ferroelectricity.

APPENDIX A: DETAILS OF OUR EXPERIMENT

To evaluate the pure electronic excitation energy, we perform a fitting analysis of the optical conductivity spectrum $\sigma(\omega)$, as shown in Fig. 1(d). It is well known that the reflectivity spectrum of a TMTTF (tetramethyltetrathiafulvalene) salt has a complex structure in the lower energy region which is attributed to the Fano interference originating from the electron-intramolecular vibration (EIMV) coupling between the charge-transfer (CT) transition and Raman active intramolecular vibration modes below 0.2 eV [32]. Fitting analyses based on the dimer model considering this effect have been performed [32,54,55]. In this section, we expand this method to analyze the optical spectrum. R in Fig. 5(a) shows the reflectivity spectrum of $(TMTTF)_2PF_6$ for the electric field polarized parallel to the a axis ($E \parallel a$), which
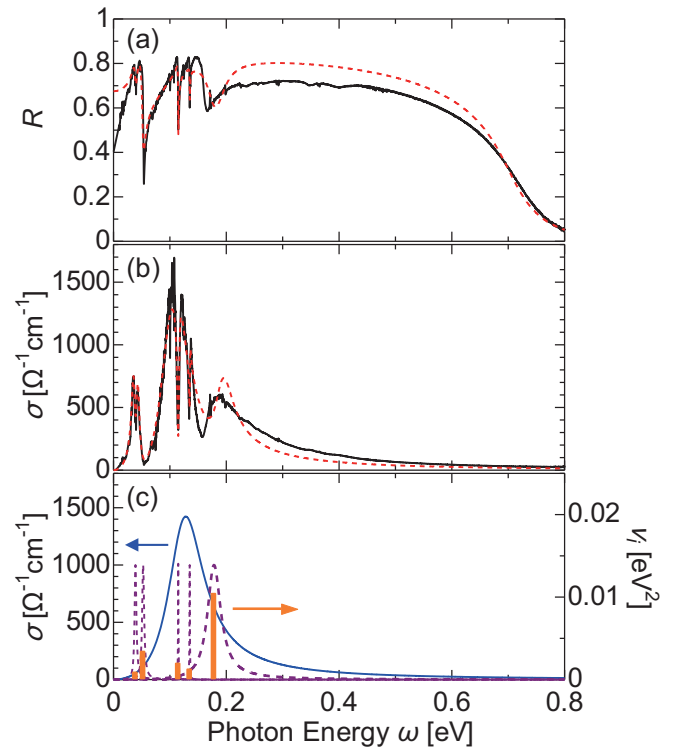

FIG. 5. (a) Polarized reflectivity and (b) optical conductivity spectrum for $E \parallel a$ at 10 K (the solid lines). The dashed lines show the fitting curves. (c) Calculated spectra of the CT transition (the solid line) and phonons (the dashed lines). The magnitude of the latter is normalized at $1000\ \Omega^{-1}cm^{-1}$. The coupling between each phonon and the CT transition is shown as a bar.

is measured by a Fourier transform infrared spectrometer. $\sigma(\omega)$ is obtained by the Kramers-Kronig transformation of the reflectivity spectrum as shown in Fig. 5(b). Considering the EIMV coupling effect in the framework of the Fano interference, we perform a fitting analysis of these spectra. The Fano interference is known to be analogous to a toy model considering classical harmonic oscillators interacting with each other [56]. In this model, the vibration modes of $(TMTTF)_2PF_6$ can be described as Fig. 6. The purely electronic CT transition without the EIMV coupling is regarded as an oscillator with charge q_{CT} and eigenfrequency ω_{CT}. In
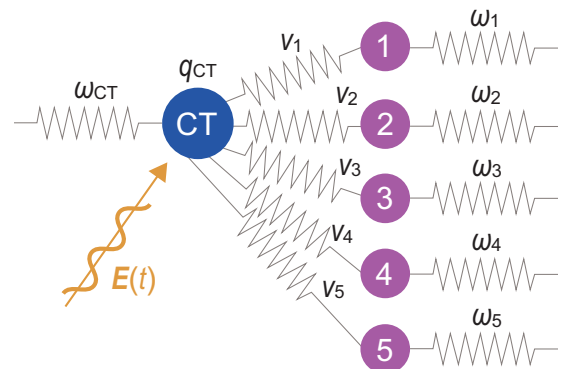

FIG. 6. Schematic of the Fano interference originating from the EIMV coupling.

TABLE I. Fitting parameters in Eq. (A3).

ε_∞	ω_{CT} [eV]	γ_{CT} [eV]	μ_{CT} [eV]
1.7	0.128	7.73×10^{-2}	0.905

j	ω_j [eV]	γ_j [eV]	ν_j [eV^2]
1	0.178	2.88×10^{-2}	1.04×10^{-2}
2	0.135	9.05×10^{-4}	1.23×10^{-3}
3	0.115	9.07×10^{-4}	1.94×10^{-3}
4	0.0525	4.30×10^{-3}	3.39×10^{-3}
5	0.0389	3.79×10^{-3}	8.67×10^{-4}

addition to this CT oscillator, infrared inactive intramolecular vibrations are introduced as oscillators j with eigenfrequencies ω_j ($j = 1, 2, 3, 4, 5$) without charges. The oscillator j is coupled with the CT oscillator via coupling constant ν_j. When a light having the electric field $E(t)$ is irradiated, only the CT oscillator is directly driven. Subsequently, the coupled vibration of the oscillator j is generated by the vibration of the CT oscillator via the EIMV coupling. This can be attributed to the infrared activation of the original infrared inactive intramolecular vibration modes due to the interaction with the CT transition.

The equation of motion for this system with external electric field $E(\omega)$ can be expressed as follows:

$$
\begin{bmatrix}
L_{CT}^{-1} & -\nu_1 & -\nu_2 & -\nu_3 & -\nu_4 & -\nu_5 \\
-\nu_1 & L_1^{-1} & 0 & 0 & 0 & 0 \\
-\nu_2 & 0 & L_2^{-1} & 0 & 0 & 0 \\
-\nu_3 & 0 & 0 & L_3^{-1} & 0 & 0 \\
-\nu_4 & 0 & 0 & 0 & L_4^{-1} & 0 \\
-\nu_5 & 0 & 0 & 0 & 0 & L_5^{-1}
\end{bmatrix}
\begin{bmatrix}
x_{CT} \\ x_1 \\ x_2 \\ x_3 \\ x_4 \\ x_5
\end{bmatrix}
=
\begin{bmatrix}
q_{CT} \\ 0 \\ 0 \\ 0 \\ 0 \\ 0
\end{bmatrix}
E(\omega),
$$

$$
L_{CT}^{-1} = \omega_{CT}^2 - \omega^2 - i\omega\gamma_{CT}, \quad L_j^{-1} = \omega_j^2 - \omega^2 - i\omega\gamma_j,
$$
(A1)

where x_{CT}, x_j denote the displacements of the CT oscillator and oscillators j, respectively. From Eq. (A1),

$$
x_{CT} = \frac{q_{CT} L_{CT}}{1 - L_{CT} D} E(\omega) \quad \left(D = \sum_{j=1}^{5} \nu_j^2 L_j \right)
$$
(A2)

is derived. Consequently, the dielectric function, including fitting parameters, can be expressed as

$$
\varepsilon(\omega) = \varepsilon_\infty + \frac{\mu_{CT}^2 L_{CT}}{1 - L_{CT} D}.
$$
(A3)

Here, μ_{CT} is a parameter proportional to q_{CT}, corresponding to the transition intensity. ε_∞ denotes the dielectric function of the background.

The reflectivity and optical conductivity spectra are calculated by $\varepsilon(\omega)$ in Eq. (A3). Measured reflectivity R and $\sigma(\omega)$ in Fig. 5 are well reproduced by the fitting curves (the dashed lines). The fitting parameters are listed in Table I. The calculated spectra of the CT transition and phonons are displayed in Fig. 5(c). From the fitting analysis, the excitation energy of the pure electronic CT excitation, ω_{CT}, is evaluated to be 0.128 eV. The discrepancy between the experimental and

calculated spectra in the higher energy region of $\sigma(\omega)$ is probably caused by the higher complexity of the spectral shape of the pure electronic CT transition than that of the single Lorentz oscillator assumed in this model. This is consistent with the result of our work indicating that photoexcited states are collective modes of charges.

APPENDIX B: SUPPLEMENTAL MATERIALS ON THEORIES

Before discussing the main subject of this section, we newly introduce parts of the model Hamiltonian and physical quantities. Here we consider N_s sites of a one-dimensional (1D) chain model with a quarter-filled hole system and an equal population of spins ($N_\uparrow = N_\downarrow = N_s/4$) at absolute zero temperature again. In addition to Eqs. (1)–(3), we newly define parts of the model Hamiltonian as follows:

$$
H_{eff}^{even} = V_{eff} \sum_{j:even} n_j, \quad H_{eff}^{odd} = V_{eff} \sum_{j:odd} n_j.
$$
(B1)

In this section, the Hamiltonian $H_t + H_{Coulomb} + H_{eff}^{even}$ is the same as H in Eq. (1) with $V_{edge} = 0$. Using the given Hamiltonian $\mathcal{H}$ and the charge-current operator J in Eq. (5), the reduced optical conductivity of given photon energy $\omega > 0$ is written as

$$
\sigma_{1R}(\omega) = -\frac{1}{N_s} \text{Im} \left[\langle \psi_0 | J \frac{1}{\omega + i\eta + E_0 - \mathcal{H}} J | \psi_0 \rangle \right]
$$
(B2)

within the framework of the linear response theory for $\eta \to 0+$. Parameters with $V_{eff} \neq 0$ in previous sections (namely, $t_1/t_2 = 0.882$, $U/t_2 = 5.230$, $V/t_2 = 3.138$, and $\eta/t_2 = 0.05$ for $t_2 = 0.1912$ eV [16,35,36]) are utilized for all the computations in this section.

In this section, all the calculations are performed by the exact diagonalization (ED) method under the periodic boundary condition (PBC) to avoid the edge effects that typically occur under the open boundary condition (OBC). Because the ED calculations are limited to a small system size of the order of $N_s \sim 20$ for the computational problem, the edge effects significantly affect the calculations and so, should be eliminated. In contrast to the density-matrix renormalization group (DMRG) [38] and dynamical DMRG (DDMRG) [37] methods in previous sections, the ED method for a fixed system size can easily yield the wave functions of arbitrary quantum states and allow their comparison owing to the unused renormalized Hamiltonians, even if the calculations involve different physical parameters. This is the reason why we select the ED method in this section.

1. Estimation of V_{eff}

The aim of this section is to discuss one of the origins of $V_{eff} = 0.086t_2$ in previous sections. As mentioned already, an unconventional term, V_{eff}, is introduced for reproducing the experimental data and indeed, several origins of V_{eff} such as the quasi-two-dimensional effects from the Coulomb interactions between 1D chains are possibly considered. However, here we consider that one of the candidates for the origin of V_{eff} is the electron-intramolecular vibration (EIMV) coupling, which is one of the effective electron-phonon coupling models
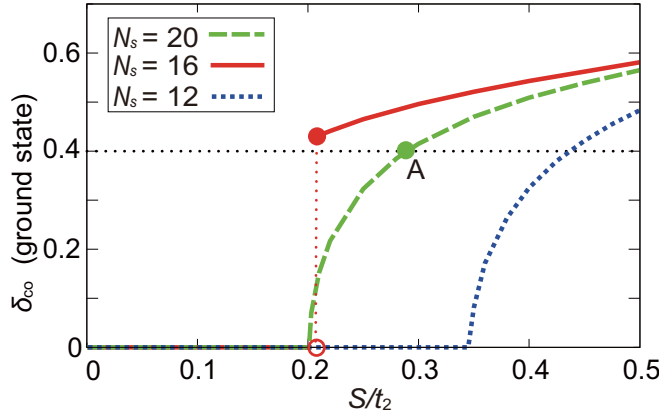
FIG. 7. Calculations of δ_{co} for S/t_2 determined by minimizing E_0^{EIMV} in Eq. (B8) for $N_s = 12, 16, 20$ with the ED method under the PBC. The horizontal dotted line and point A correspond to $\delta_{co} = 0.40$ [25].

[47–49]. Using Eqs. (2) and (3), our starting Hamiltonian, H_{eph}, is written as

$$H_{eph} \equiv H_t + H_{Coulomb} + H_{EIMV}, \tag{B3}$$

$$H_{EIMV} = -\sum_{\alpha,j} S_\alpha x_j^\alpha n_j + \sum_{\alpha,j} \frac{S_\alpha}{2}(x_j^\alpha)^2, \tag{B4}$$

where x_j^α denotes the dimensionless reference frame of molecular vibration mode α at the jth site. For a certain vibration mode α, we represent g_α as an EIMV coupling constant and Ω_α as a frequency of a molecular vibration, respectively. Then $S_\alpha = 2g_\alpha^2/\Omega_\alpha$. Here, we introduce the mean fields of charge disproportion δ_{co} and amplitude of the molecular vibration x_0^α as follows:

$$\langle \psi_0 | n_j | \psi_0 \rangle = \frac{1}{2} + (-1)^{j-1} \frac{\delta_{co}}{2}, \tag{B5}$$

$$x_j^\alpha = (-1)^{j-1} x_0^\alpha. \tag{B6}$$

After considering the appropriate constant energy shift and comparing H_{eph} in Eq. (B3) with $H_t + H_{Coulomb} + H_{eff}^{even}$ [see Eqs. (2), (3), and (B1)], which is the same as H in Eq. (1) with $V_{edge} = 0$,

$$V_{eff} = \sum_\alpha S_\alpha \delta_{co} \tag{B7}$$

is derived by the Hellmann-Feynman theorem. In the charge-ordered (CO) ground state, because a finite δ_{co} deforms the molecular orbitals associated with n_j for each site, V_{eff} in Eq. (B7) can be interpreted as an effective potential representing such deformation.

To simplify the problem, we select a single molecular vibration mode, β ($S_\alpha = 0, x_j^\alpha = 0$ for $\alpha \neq \beta$), and define $S_\beta \equiv S$, $x_j^\beta \equiv x_0$. Then, we can derive $x_0 = \delta_{co}/2$ similarly as discussed above. δ_{co} for a fixed S/t_2 is determined by minimizing the ground-state energy E_0^{EIMV} written as

$$E_0^{EIMV} = \langle \psi_0 | H_{eph} | \psi_0 \rangle \quad (x_0 = \delta_{co}/2). \tag{B8}$$

Within the framework of the ED calculation under the PBC, the results of δ_{co} for $N_s = 12, 16,$ and 20 are shown in Fig. 7.

To avoid the finite-size effect, we use the result for $N_s = 20$, which is the largest system size in our calculations, and estimate V_{eff}.

In a recent experiment [25], because $\delta_{co} = 0.40$ was observed in the CO ground state at 30 K, $V_{eff} = S\delta_{co} \sim 0.116t_2 \equiv V_{eff}^{ED}$ could be estimated at $\delta_{co} = 0.40$ by using value $S/t_2 = 0.291$ for $N_s = 20$ at point A, as shown in Fig. 7. The estimated value of V_{eff}^{ED} is close to $V_{eff} = 0.086t_2$.

Apart from the structural similarity to the first-order phase transition seen in Fig. 7, the value S/t_2 vanishes δ_{co} of $N_s = 16$ and that of $N_s = 20$ are quantitatively regarded as practically unchanged. Therefore, our ED calculations presented in the next section focus on $N_s = 16$.

Here, we briefly comment on the origin of the first-order phase transition noted in Fig. 7. According to the observed T-P phase diagram of (TMTTF)$_2$PF$_6$ [10], the spin-Peierls (SP) phase should be the ground state at $T = 0$ and, in general, it should have both $4k_F$-charge density wave (CDW) and $2k_F$-spin density wave (SDW) instabilities [57], where k_F denotes
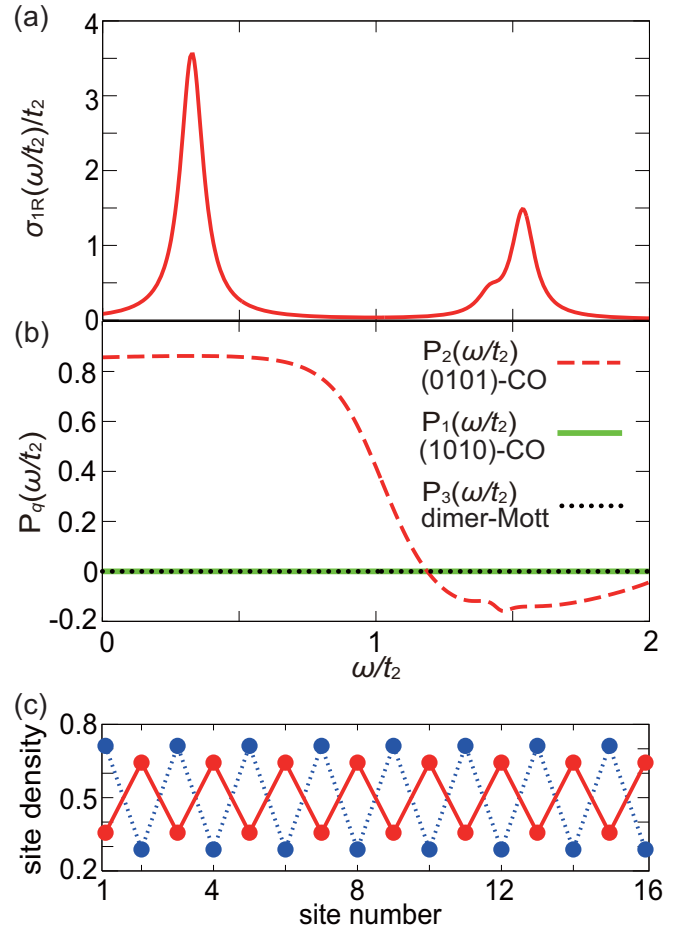

FIG. 8. Calculations by the ED method under the PBC for $N_s = 16, \eta/t_2 = 0.05$. (a) Computed $\sigma_{1R}(\omega/t_2)$ of H_1 in Eq. (B9). (b) Projections of a state, $|\Phi_1(\omega)\rangle$, onto the ground states at different physical phases $|\Psi_1\rangle$ ((1010)-CO), $|\Psi_2\rangle$ ((0101)-CO), and $|\Psi_3\rangle$ (dimer-Mott). (c) Site densities. The solid line connected with solid circles describes the site density of the photoexcited state at the first peak of $\sigma_{1R}(\omega/t_2)$ shown in (a). For comparison, the site density of the ground state is displayed as a dotted line with filled circles.

a Fermi wave number. In this section, we only set the CO mean field δ_{co} that has a $4k_F$ instability and do not treat the $2k_F$ instability of an antiferromagnetic order appearing in the SP state. Consequently, a tetrameric model should be considered for ensuring the second-order phase transition of δ_{co}, which is our future work.

2. Dimer-Mott state in the excited state

In this section, we investigate the relationship between the dimer-Mott (DM) state and the photoexcited state by means of the ED method under the PBC. All the calculations are conducted at $N_s = 16$, as discussed in the previous section. In addition, we also inquire regarding the existence of the polarization (P)-inverted CO state in the photoexcited state for comparison. For this purpose, using Eqs. (2), (3), and (B1) we introduce three Hamiltonians defined as

$$H_1 \equiv H_t + H_{Coulomb} + H_{eff}^{even}, \qquad (B9)$$

$$H_2 \equiv H_t + H_{Coulomb} + H_{eff}^{odd}, \qquad (B10)$$

$$H_3 \equiv H_t + H_{Coulomb}(V = 0). \qquad (B11)$$

From the discussions in previous sections, because H_1 in Eq. (B9) corresponds to the original Hamiltonian H with $V_{edge} = 0$ in Eq. (1), the ground state of H_1 in Eq. (B9), defined as $|\Psi_1\rangle$, is rich in charges on every odd site, and we symbolically represent this as "(1010)-CO." In contrast, we define $|\Psi_2\rangle$ as the ground state of H_2 in Eq. (B10) and $|\Psi_2\rangle$ as having rich charges on each even site, which we symbolically represent as "(0101)-CO." This state can be ascribed as a P-inverted CO state with respect to $|\Psi_1\rangle$. The DM ground state $|\Psi_3\rangle$ considers the ground state of H_3 in Eq. (B11), and we simply refer to $|\Psi_3\rangle$ as a "dimer-Mott." Although

some theoretical works have revealed the phase diagram of the ground state in a 1D quarter-filled Hamiltonian $H_t + H_{Coulomb}$ [see Eqs. (2) and (3)] and the parameter region of the DM phase with nonvanishing U and V [16,36], we particularly choose $V = 0$ in H_3 [Eq. (B11)] for completely neglecting the charge-ordering effects originating from $V \neq 0$.

We calculate a photoexcited state with given photon energy ω and J in Eq. (5) as

$$|\Phi_1(\omega)\rangle \equiv \frac{1}{\mathcal{N}_1} \frac{\eta}{(\omega - E_1 + H_1)^2 + \eta^2} J|\Psi_1\rangle, \qquad (B12)$$

where E_1 represents the ground-state energy of H_1 in Eq. (B9). $\mathcal{N}_1$ is determined by satisfying $1 = \langle\Phi_1(\omega)|\Phi_1(\omega)\rangle$. In addition to this, we also calculate

$$P_q(\omega) \equiv \langle\Psi_q|\Phi_1(\omega)\rangle \quad (q = 1, 2, 3), \qquad (B13)$$

which denotes the characteristic quantities for qualitatively estimating the mixing degrees of the different ground states $|\Psi_{q=1,2,3}\rangle$ with respect to $|\Phi_1(\omega)\rangle$.

$\sigma_{1R}(\omega/t_2)$ with $\mathcal{H} = H_1$, $E_0 = E_1$, and $|\psi_0\rangle = |\Psi_1\rangle$ in Eq. (B2) is shown in Fig. 8(a). Our calculations of $P_{q=1,2,3}(\omega)$ are displayed in Fig. 8(b). $V_{eff}/t_2 = 0.086$ is chosen for the calculations presented here. These values also allow discussing the same photoexcitation calculated under the OBC in the previous sections except for finite-size effects. As can be seen, in addition to the obvious result of $P_1(\omega) = 0$, it is clear that $P_2(\omega) \neq 0$ and $P_3(\omega) = 0$. In particular, $P_2(\omega) \sim 1$ can be seen around the first peak of $\sigma_{1R}(\omega/t_2)$. Therefore, the photoexcited state at the first peak is highly inclusive of the P-inverted state, $|\Psi_2\rangle$ [(0101)-CO], regarding the $|\Psi_1\rangle$ [(1010)-CO] ground state, but it is exclusive of the DM state, $|\Psi_3\rangle$. Compared to the site density of the ground state $\langle\Psi_1|n_j|\Psi_1\rangle$, the enhancement of the "(0101)-CO" photoexcited state at the first peak is consistent with site density at the peak $\langle\Phi_1(\omega)|n_j|\Phi_1(\omega)\rangle$ shown in Fig. 8(c).

[1] H. Okamoto, Ultrafast photoinduced phase transitions in one-dimensional organic correlated electron systems, *Molecular Electronic and Related Materials-Control and Probe with Light* (Transworld Research Network, Kerala, India, 2010), pp. 59–97.

[2] D. N. Basov, R. D. Averitt, D. van der Marel, M. Dressel, and K. Haule, Rev. Mod. Phys. **83**, 471 (2011).

[3] S. Iwai, K. Yamamoto, A. Kashiwazaki, F. Hiramatsu, H. Nakaya, Y. Kawakami, K. Yakushi, H. Okamoto, H. Mori, and Y. Nishio, Phys. Rev. Lett. **98**, 097402 (2007).

[4] K. Yamamoto, S. Iwai, S. Boyko, A. Kashiwazaki, F. Hiramatsu, C. Okabe, N. Nishi, and K. Yakushi, J. Phys. Soc. Jpn. **77**, 074709 (2008).

[5] H. Yamakawa, T. Miyamoto, T. Morimoto, H. Yada, Y. Kinoshita, M. Sotome, N. Kida, K. Yamamoto, K. Iwano, Y. Matsumoto, S. Watanabe, Y. Shimoi, M. Suda, H. M. Yamamoto, H. Mori, and H. Okamoto, Sci. Rep. **6**, 20571 (2016).

[6] T. Luty, H. Cailleau, S. Koshihara, E. Collet, M. Takesada, M. H. L.- Cailleau, M. B.- Le Cointe, N. Nagaosa, Y. Tokura,

E. Zienkiewicz, and B. Ouladdiaf, Europhys. Lett. **59**, 619 (2002).

[7] K. Iwano, Y. Shimoi, T. Miyamoto, D. Hata, M. Sotome, N. Kida, S. Horiuchi, and H. Okamoto, Phys. Rev. Lett. **118**, 107404 (2017).

[8] K. Yonemitsu, Crystals **2**, 56 (2012).

[9] B. Salameh, S. Yasin, M. Dumm, G. Untereiner, L. Montgomery, and M. Dressel, Phys. Rev. B **83**, 205126 (2011).

[10] B. Köhler, E. Rose, M. Dumm, G. Untereiner, and M. Dressel, Phys. Rev. B **84**, 035124 (2011).

[11] K. Medjanik, M. de Souza, D. Kutnyakhov, A. Gloskovskii, J. Müller, M. Lang, J.-P. Pouget, P. F. -Leylekian, A. Moradpour, H.-J. Elmers, and G. Schönhense, Eur. Phys. J. B **87**, 256 (2014).

[12] S. Tomić and M. Dressel, Rep. Prog. Phys. **78**, 096501 (2015).

[13] I. Voloshenko, M. Herter, R. Beyer, A. Pustogow, and M. Dressel, J. Phys.: Condens. Matter **29**, 115601 (2017).

[14] H. Wilhelm, D. Jaccard, R. Duprat, C. Bourbonnais, D. Jérome, J. Moser, C. Carcel, and J. M. Fabre, Eur. Phys. J. B **21**, 175 (2001).

[15] L. Degiorgi and D. Jérome, J. Phys. Soc. Jpn. **75**, 051004 (2006).

[16] H. Seo, J. Merino, H. Yoshioka, and M. Ogata, J. Phys. Soc. Jpn. **75**, 051009 (2006).

[17] F. Iwase, K. Sugiura, K. Furukawa, and T. Nakamura, J. Phys. Soc. Jpn. **78**, 104717 (2009).

[18] H. Seo and H. Fukuyama, J. Phys. Soc. Jpn. **66**, 1249 (1997).

[19] D. S. Chow, F. Zamborszky, B. Alavi, D. J. Tantillo, A. Baur, C. A. Merlic, and S. E. Brown, Phys. Rev. Lett. **85**, 1698 (2000).

[20] P. Monceau, F. Y. Nad, and S. Brazovskii, Phys. Rev. Lett. **86**, 4080 (2001).

[21] M. Dressel, M. Dumm, T. Knoblauch, and M. Masino, Crystals **2**, 528 (2012).

[22] M. de Souza, L. Squillante, C. Sônego, P. Menegasso, P. Foury-Leylekian, and J. P. Pouget, Phys. Rev. B **97**, 045122 (2018).

[23] A. Pustogow, T. Peterseim, S. Kolatschek, L. Engel, and M. Dressel, Phys. Rev. B **94**, 195125 (2016).

[24] R. Świetlik, B. Barszcz, A. Pustogow, and M. Dressel, Phys. Rev. B **95**, 085205 (2017).

[25] S. Kitou, T. Fujii, T. Kawamoto, N. Katayama, S. Maki, E. Nishibori, K. Sugimoto, M. Takata, T. Nakamura, and H. Sawa, Phys. Rev. Lett. **119**, 065701 (2017).

[26] K. Iwano, Phys. Rev. Lett. **97**, 226404 (2006); **102**, 106405 (2009); Phys. Rev. B **91**, 115108 (2015).

[27] M. Mayr and P. Horsch, Phys. Rev. B **73**, 195103 (2006).

[28] K. Onda, S. Ogihara, K. Yonemitsu, N. Maeshima, T. Ishikawa, Y. Okimoto, X. Shao, Y. Nakano, H. Yamochi, G. Saito, and S. Y. Koshihara, Phys. Rev. Lett. **101**, 067403 (2008).

[29] H. Hashimoto, H. Matsueda, H. Seo, and S. Ishihara, J. Phys. Soc. Jpn. **83**, 123703 (2014).

[30] V. Vescoli, L. Degiorgi, W. Henderson, G. Grüner, K. P. Starkey, and L. K. Montgomery, Science **281**, 1181 (1998).

[31] M. Dumm, M. Abaker, M. Dressel, and L. K. Montgomery, J. Low Temp. Phys. **142**, 613 (2006).

[32] Y. Naitoh, Y. Kawakami, T. Ishikawa, Y. Sagae, H. Itoh, K. Yamamoto, T. Sasaki, M. Dressel, S. Ishihara, Y. Tanaka, K. Yonemitsu, and S. Iwai, Phys. Rev. B **93**, 165126 (2016).

[33] T. Nakamura, J. Phys. Soc. Jpn. **72**, 213 (2003).

[34] T. Nakamura, K. Furukawa, and T. Hara, J. Phys. Soc. Jpn. **76**, 064715 (2007).

[35] A. C. Jacko, H. Feldner, E. Rose, F. Lissner, M. Dressel, R. Valentí, and H. O. Jeschke, Phys. Rev. B **87**, 155139 (2013).

[36] M. Tsuchiizu, H. Yoshioka, and Y. Suzumura, J. Phys. Soc. Jpn. **68**, 1809 (1999); **70**, 1460 (2001).

[37] E. Jeckelmann, Phys. Rev. B **66**, 045114 (2002).

[38] S. R. White, Phys. Rev. Lett. **69**, 2863 (1992); Phys. Rev. B **48**, 10345 (1993).

[39] M. Vekić and S. R. White, Phys. Rev. Lett. **71**, 4283 (1993).

[40] A. Gendiar, R. Krcmar, and T. Nishino, Prog. Theor. Phys. **122**, 953 (2009).

[41] N. Shibata and C. Hotta, Phys. Rev. B **84**, 115116 (2011).

[42] S. R. White and D. A. Huse, Phys. Rev. B **48**, 3844 (1993).

[43] H. Benthien and E. Jeckelmann, Eur. Phys. J. B **44**, 287 (2005).

[44] F. Mila, Phys. Rev. B **52**, 4788 (1995).

[45] L. Ducasse, M. Abderrabbat, J. Hoaraut, M. Pesquert, B. Gallois, and J. Gaultier, J. Phys. C: Solid State Phys. **19**, 3805 (1986).

[46] G. Giovannetti, S. Kumar, J.-P. Pouget, and M. Capone, Phys. Rev. B **85**, 205146 (2012).

[47] M. J. Rice, Solid State Commun. **31**, 93 (1979).

[48] K. Nasu, J. Phys. Soc. Jpn. **53**, 302 (1984).

[49] A. Painelli and A. Girlando, J. Chem. Phys. **84**, 5655 (1986).

[50] T. Umanodan, S. Tanaka, S. Naruse, T. Ishikawa, K. Onda, S. Koshihara, S. Horiuchi, and Y. Okimoto, J. Phys. Soc. Jpn. **84**, 073707 (2015).

[51] N. Ikeda, H. Ohsumi, K. Ohwada, K. Ishii, T. Inami, K. Kakurai, Y. Murakami, K. Yoshii, S. Mori, Y. Horibe, and H. Kito, Nature (London) **436**, 1136 (2005).

[52] K. Kobayashi, S. Horiuchi, R. Kumai, F. Kagawa, Y. Murakami, and Y. Tokura, Phys. Rev. Lett. **108**, 237601 (2012).

[53] T. Miyamoto, H. Yada, H. Yamakawa, and H. Okamoto, Nat. Commun. **4**, 2586 (2013).

[54] M. J. Rice, V. M. Yartsev, and C. S. Jacobsen, Phys. Rev. B **21**, 3437 (1980).

[55] C. S. Jacobsen, D. B. Tanner, and K. Bechgaard, Phys. Rev. B **28**, 7019 (1983).

[56] Y. S. Joe, A. M. Satanin, and C. S. Kim, Phys. Scr. **74**, 259 (2006).

[57] J. E. Hirsch and D. J. Scalapino, Phys. Rev. Lett. **50**, 1168 (1983); Phys. Rev. B **27**, 7169 (1983); **29**, 5554 (1984).